Ultrasonics Sonochemistry 111 (2024) 107131

Contents lists available at ScienceDirect

Ultrasonics Sonochemistry

journal homepage: www.elsevier.com/locate/ultson

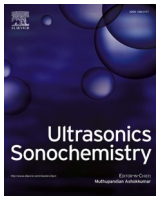

Antimicrobial and antifouling hyaluronic acid-cobalt nanogel coatings built sonochemically on contact lenses

Guillem Ferreres [a], Sílvia Pérez-Rafael [a], Ester Guaus [a], Òscar Palacios [b], Ivan Ivanov [a], Juan Torrent-Burgués [a], Tzanko Tzanov [a,*]

[a] Grup de Biotecnologia Molecular i Industrial, Department of Chemical Engineering, Universitat Politècnica de Catalunya, Rambla Sant Nebridi 22, Terrassa 08222, Spain

[b] Departament de Química, Facultat de Ciències, Universitat Autònoma de Barcelona, 08193 Barcelona, Bellaterra, Spain

ARTICLE INFO

Keywords:
Contact lenses
Sonochemical coating
Hyaluronic acid
Cobalt
Metal–organic complex
Antibacterial

ABSTRACT

The wearing of contact lenses (CLs) may cause bacterial infections, leading in turn to more serious complications and ultimately vision impairment. In this scenario, the first step is the adhesion of tear proteins, which provide anchoring points for bacterial colonization. A possible solution is the functionalization with an antimicrobial coating, though the latter may also lead to sight obstruction and user discomfort. In this study, adipic acid dihydrazide-modified hyaluronic acid-cobalt (II) (HA-ADH-Co) nanogels (NGs) were synthesized and deposited onto commercial CLs in a single-step sonochemical process. The coating hindered up to 60 % the protein adsorption and endowed the CLs with strong antibacterial activity against major ocular pathogens like *Staphylococcus aureus* and *Pseudomonas aeruginosa*, reducing their concentration by around 3 logs. Cytotoxicity assessment with human corneal cells demonstrated viabilities above 95 %. The nanocomposite coating did not affect the optical power and the light transmission of the CLs and provided enhanced wettability, important for the wearer comfort.

1. Introduction

Contact lenses (CLs) are commonly used to correct vision and their use has expanded to other applications such as post-operative ocular discomfort treatment and drug delivery [1–3]. Modern CLs are primarily based on silicone hydrogels that, along superior mechanical properties, combine wettability (related to user comfort) with adequate oxygen permeability (to ensure proper corneal metabolism) [4–7]. Despite of the high hydrophilicity of these materials, tear proteins comprising lysozyme, lactoferrin, lipocalin, and IgA aggregate on the CL surface, causing discomfort, vision impairment, and increased risk of bacterial colonization, especially when proper lens hygiene is not maintained [8,9]. Ocular surface infections associated with *Pseudomonas aeruginosa*, *Staphylococcus aureus*, *Enterobacteriaceae* spp., *Corynebacterium* spp., and *Propionibacterium* spp. may deteriorate to keratitis, the fifth leading cause for blindness, which condition is largely predisposed by wearing of CLs [10,11].

Traditionally, ocular bacterial infections are treated with topically applied broad-spectrum antibiotics, however, the efficacy of the latter is compromised by the rapid appearance of antimicrobial resistance (AMR) as a result from the overuse and misuse of antibiotics [12]. Thus, alternative strategies for the prevention of CL-related infections (and AMR in general) are sought, e.g., by using antibiotic-free antimicrobials on the material surface or impregnated in the material bulk. Some examples of surface treatments are the deposition of free radical-generating organo-selenium compounds, antimicrobial peptides, or quorum-sensing inhibitors [13–15]. However, major limitations of these approaches are related to coloration of the lens, low stability of the coating, wearer discomfort, and overall deterioration of the optical properties [16].

Metal nanoparticles (NPs) or metal–organic complexes coated on the surface is another efficient antimicrobial and antifouling strategy, whereby the coating stability may be achieved by chemical or physical crosslinking [17–19]. Chemical crosslinking, however, usually necessitates harsh chemicals, while the reversible character of physical adsorption may compromise the durability. In this regard, high-intensity ultrasonic (US) treatment is a versatile waterborne approach for material-independent surface functionalization. This process has been in

* Corresponding author.
E-mail address: tzanko.tzanov@upc.edu (T. Tzanov).

https://doi.org/10.1016/j.ultsonch.2024.107131
Received 12 June 2024; Received in revised form 20 September 2024; Accepted 24 October 2024
Available online 28 October 2024

fact upvoted by IUPAC as a top-ten emerging technology in 2021, highlighting the durability of antibacterial textile coatings [20]. The cavitation phenomenon during sonication generates microjets that project dissolved or colloidal materials towards the surface, resulting in more stable coatings. This technology has been applied for deposition of zinc-doped copper oxide NPs, zinc oxide NPs combined with gallic acid and tobramycin, as well as for hybrid coatings of chitosan, gallic acid, and zinc oxide NPs on CLs to prevent bacterial colonization [21–23]. Despite the proven antimicrobial efficacy of these NPs, they may potentially cause human and environmental toxicity upon release [24,25].

On the other hand, antimicrobial metals such as cobalt that have lower toxicity are already being used in implants and medical treatments [26–28]. Antimicrobial cobalt-organic NPs have shown potential against multiple pathogens like bacteria, fungi, and viruses [29]. Although cobalt is an essential trace element for many organisms, including humans, high concentrations or prolonged exposure to cobalt can lead to adverse effects that need to be mitigated in the case of biomedical use [30]. Combining cobalt ions with organic ligands may enhance the antimicrobial performance of these NPs while improving their safety. For example, natural polymers like hyaluronic acid (HA) have been used to increase the biocompatibility of otherwise toxic active agents [31,32]. HA has been functionalized to design composite materials for different biomedical applications in form of hydrogels, NPs, or nanogels (NGs) [33,34]. NGs in particular feature high water absorption and water retention capacity that, coupled with the moisturizing function of HA, makes them suitable for ophthalmological applications, enhancing eye hydration and lubrication, while preventing irritation [35–37].

The current work developed biocompatible antibacterial coating on CLs that maintained both the wearer comfort and the optical properties of the material. To this end, first, modification of HA with the chelator adipic acid dihydrazide (ADH) led to the formation of complex with cobalt(II), which enabled controlled ion release alongside the recognized ophthalmological benefits of HA. Afterwards, the HA-ADH-Co NGs were simultaneously synthesized and deposited on the surface using sonochemistry, significantly reducing the environmental footprint of the process, compared to other functionalization approaches. The rationale behind this approach was to use said hybrid NGs to prevent protein adsorption and subsequent bacterial colonization, where HA would ensure biocompatibility and wettability of the device. To prove their efficacy, the nanocomposite coatings were validated with major eye pathogens, *P. aeruginosa* and *S. aureus*, while assessing the biocompatibility with human corneal cells. Furthermore, functional tests of the comfort-related and optical properties added up to a comprehensive characterization towards practical feasibility.

2. Materials and methods

2.1. Reagents

Comfilcon A (silicone-hydrogel) CL (dry dioptric power (PWRd): −5.00 D and nominal water content: 48 %) were purchased from Coopervision (USA). Pharmaceutical grade hyaluronic acid (HA) sodium salt from *Streptococcus Equi* (MW = 40 kDa) was obtained from Lehvoss Iberia (Spain). Adipic acid dihydrazide (ADH), phosphate buffer saline (PBS) tablets, 1-ethyl-3-(3-dimethylaminopropyl)carbodiimide (EDC), hydrochloric acid, nitric acid, Bradford dye reagent, iodonitrotetrazolium chloride, 98 % were provided by Thermo Fischer Scientific (Spain). Cobalt(II) nitrate hexahydratate, Muller-Hinton Broth (MHB), Dulbecco's Modified Eagle's Medium – high glucose (DMEM), and LB agar, were supplied by Sigma-Aldrich (Spain). Invitrogen Life Technologies Corporation (Spain) supplied the alamarBlue cell viability reagent. The American Type Culture Collection (ATCC LGC Standards, Spain) provided the bacterial strains *Staphylococcus aureus* (ATCC 25923) and *Pseudomonas aeruginosa* (ATCC 10 145). Human corneal epithelial (HCE) cells H-6048IM were supplied by Quimigen (Spain). Avanti Polar Lipids, Inc. (Alabama, USA) supplied phosphatidylethanolamine (PE) and phosphatidylglycerol (PG), extracted from *Escherichia coli*.

2.2. Synthesis of HA-ADH

The HA modification was performed following a reported protocol [38]. Briefly, HA was dissolved in MilliQ water to a final concentration of 2.5 mg/mL. After the complete dissolution of the polymer, ADH was introduced in the solution at a concentration of 45-fold molar excess. The pH was adjusted to 4.8 using 1 M HCl following 30 min incubation. Then, a 4-fold molar excess of EDC was added to the mixture, and the solution pH was adjusted to 4.8 every 15 min. After 2 h, the reaction was stopped by raising the pH to 7.0 with 1 M NaOH. The HA-ADH was dialyzed four times using distilled water (3 h incubation and a final one overnight). The modified polymer was freeze-dried for 3 days and stored at 4 °C in a nitrogen atmosphere. Fourier-transform infrared spectroscopy (FTIR) was performed to confirm the modification of the polymer using a PerkinElmer Spectrum 100 (PerkinElmer, USA). The baseline correction and the spectra were normalized using the maximum absorbance at 1030 cm^{-1} using the PerkinElmer Spectrum software.

2.3. NGs synthesis and characterization

First, a 15 mL 0.5 % (w/v) solution of HA modified with ADH was prepared at in MilliQ water and added dropwise to a 15 mL 1 % (w/v) cobalt nitrate pH 9 Tris buffer solution. The mixture was stirred for 30 min to allow the formation of the complex. After that, the modified hyaluronic acid-cobalt (HA-ADH-Co) complex was centrifuged for 1 min at 1000 × *g* and separated from the water fraction. The pellet was washed twice to remove the unreacted precursors, and the HA-ADH-Co complex was dispersed in MilliQ water and centrifuged at the aforementioned conditions, followed by sonication using a high-intensity Vibra-Cell VCX 750 ultrasonic processor (Sonics and Materials, Inc., USA) with a 20 kHz Ti horn during 30 min at 35 % amplitude to allow its fragmentation into NGs. The freeze-dried NGs were analyzed by FTIR as described above. Co2p, N1s, O1s, and C1s (as reference) X-ray photoelectron spectroscopy (XPS) spectra were recorded at pass energy of 25 eV in ultra-high vacuum ($5.0 \cdot 10^{-9}$ mbar) using a Phoibos 150 MCD-9 detector and a XR50 Mg anode source working at 150 W (D8 advance, SPECS Surface Nano Analysis GmbH, Germany). The morphology of the NGs was assessed by scanning electron microscopy (SEM), whereby the nanostructures were sputtered with gold/palladium coating and observed by a field-emission SEM (Merlin Zeiss, Germany) operating at 2 kV. To confirm the hydrogel-like behavior of the NGs, the changes in their hydrodynamic diameter were assessed at temperatures from 10 to 50 °C employing a Zetasizer Nano ZS (Malvern Instruments Inc., U.K.).

2.4. Antimicrobial activity of the NGs

In order to test the antimicrobial activity of the NGs in colloid form, *S. aureus and P. aeruginosa* were growth for 24 h overnight in Lysogeny broth (LB) at 37 °C. The cultures were diluted until reaching an optical density (OD) at λ = 600 nm (OD_{600}) of 0.01 (equivalent to approximately 10^5–10^6 colony forming units (CFU) per mL). 50 μL of this bacterial culture were mixed with the same volume of various concentrations of NGs and incubated for 24 h at 37 °C with shaking at 230 rpm. Serial dilutions of the bacterial cultures were plated onto LB agar plates, which were subsequently incubated for an additional 24 h at 37 °C. Finally, the colonies were counted to assess the number of surviving bacteria. The log reduction of each NPs concentration was calculated regarding the concentration of the bacteria at the start of the experiment.

2.5. Antibacterial mechanism of the NGs

First, the interactions of NGs with a model membrane were assessed by surface pressure-area isotherms. Monolayers of phospholipids were formed using a chloroform solution of 0.4 mg/mL of PE and 0.1 mg/mL of PG employing a 100 mM pH 7.4 PBS or NGs diluted in PBS subphases in a Langmuir trough (KSV NIMA Langmuir–Blodgett Deposition Troughs) equipped with two mobile barriers inside an insulation box at 23 ± 1 °C secured on an antivibration table. The measurements of the surface pressure (π) were carried out with a Wilhelmy balance connected to the trough. The system was washed two times with chloroform followed by several washes with water until the pristine subphase displayed a negligible surface pressure. Thereafter, the subphases were added to the system and stabilized for 30 min, before the addition of 30 μL of the phospholipid mixture on their surface. The chloroform was evaporated for 10 min before the start of the recording. The closing rate of the barriers was set at 15 cm^2/min.

In order to evaluate the impact of NGs on the bacterial electron transport chain, the dehydrogenase activity was assessed. 250 μL of *S. aureus* or *P. aeruginosa* cultures at an OD_{600} of 0.2 were incubated with 250 μL of HA-ADH-Co NGs for 2 h. After incubation, the cells were centrifuged at 8000 × *g* for 10 min, and the resulting pellet was washed twice with 500 μL of PBS and centrifuged again. Finally, the pellet was resuspended in 500 μL of the same buffer solution containing 0.05 % (w/v) iodonitrotetrazolium chloride. The resuspension was then kept in dark conditions for 30 min. Subsequently, the same volume of acetone: ethanol (1:1) were added to the reaction to solubilize the red precipitate and measured by UV–Vis spectroscopy at 495 nm.

2.6. Coating of contact lenses with NGs

Solution of HA modified with ADH (0.5 % w/v) was prepared in MilliQ water and added dropwise to a 1 % (w/v) cobalt nitrate solution in Tris buffer pH 9, and the mixture was stirred for 30 min to allow the formation of the complex. Thereafter, the complex was centrifuged for 1 min at 1000 × *g*, washed twice in order to remove the unreacted precursors and finally resuspended in MilliQ water. 3 CLs were sonicated in the metal–organic solution using a high-intensity Vibra-Cell VCX 750 ultrasonic processor (Sonics and Materials, Inc., USA) with a 20 kHz Ti horn during 30 min at 35 % amplitude in order to simultaneously form the nanogels (NGs) and coat them onto the surface of the silicone hydrogel. Controls were performed sonicating CLs in MilliQ water, in a 0.5 % (v/v) HA-ADH solution and 1 % (v/v) of cobalt salt solution.

2.7. Characterization of the NG coating

The morphology of the coating was assessed by SEM using the same procedure as explained above. Atomic force microscopy (AFM) in liquid tapping mode was employed to assess the topography surface of the coating using a Multimode AFM controlled by a Nanoscope electronics (Bruker, Germany). A triangular AFM probe with antimony (Sn) doped Si cantilevers and silicon tips (RTESPA-150, Bruker) was used under ambient conditions with a resonant frequency of 150 kHz and nominal spring constant of 5 N/m. The CLs were cut, glued on a poly(tetrafluoroethylene) (PTFE) surface, and attached to a metallic AFM disc. Then, 20 mL of MilliQ water were cast on the CL. The samples were thermally stabilized for 10 min and the images were obtained at 1 Hz line frequency and the sample damage was reduced using minimum vertical force. Software Nanoscope analysis v1.5 was used to process the images. The release of cobalt from the material was evaluated by incubating CLs in 1 mL of PBS pH 7.4. Samples were taken after 0.5, 1, 2, 3 and 24 h, and the extracted volume was replaced with fresh PBS. The cobalt content of the aliquots was assessed using Inductively Coupled Plasma Mass Spectrometry (ICP-MS). 0.6 mL of 20 % nitric (v/v) acid were added to each sample and incubated at 100 °C for 60 min. Then, ultrapure water was added to each sample to reach 6 mL of final volume, resulting in a final concentration of 2 % (v/v) nitric acid. Finally, the potentially remaining solids were eliminated by filtration and the cobalt content was assessed using an ICP-MS 7800 (Agilent Technologies, USA) calibrated by internal standard with ^{45}Rh and a standard curve of ^{58}Co. The oxygen transport through the material was measured by a specially adapted setup [39]. The CLs were sandwiched between two compartments containing oxygen-depleted PBS in the first one and aerated PBS in the other. The measurements were performed 20 min after mounting the setup using gold screen-printed electrode (Dropsens) and μ-Autolab potentiostat (Ecochemie, NL).

2.8. Optical and comfort characterization of the NGs coating

Before the optical measurements, the tested CLs were incubated in PBS for 24 h. The optic power measurements of the air-dried CLs were performed in an Auto Lensmeter TL-3000B (Tomey Corporation, Germany). A calibration curve was carried out using dried CLs of different optic power. The transmittance spectra of the wet CLs were recorded with a Varian Cary 100 Bio spectrophotometer (Varian, Australia) in 1 cm quartz cuvettes. After that, the changes in the hydrophilicity of the CLs were assessed. Three CL of each group were immersed in PBS and incubated overnight. Then the excess of PBS of the lenses was removed and the contact angle was measured casting a 2 μL water drop with a Drop Shape Analyzer (Krüss, Germany). Finally, the water retention of the coatings was assessed. The unbound water was gently removed with absorbent paper. After that, the CLs were incubated at 22 ± 1 °C and at a relative humidity of 35 ± 2 %. Finally, the water content and the dehydration rate were assessed gravimetrically.

2.9. Protein adsorption on the CLs surface

The CLs were incubated overnight in 1.5 mL solution of 6 mg/mL of bovine serum albumin (BSA) or 2.3 mg/mL of lysozyme in PBS for 24 h. Then, the CLs were transferred to new tubes containing 1.5 mL of fresh PBS, vortexed for 3 min and incubated for 15 min in the US bath at 35 % of amplitude in order to detach the protein from the CLs. Finally, 20 μL from each sonicated tube were transferred to 96-well plate and mixed with 200 μL of Bradford dye reagent. After 10 min of incubation, the absorbance changes were measured at 595 nm.

2.10. Bacterial adhesion on the CLs surface

The CLs were incubated in static conditions in a 24-well plates for 24 h with 1 mL of PBS containing *P. aeruginosa* or *S. aureus* at an OD_{600} = 0.005. After incubation, the CLs were washed 3 times using 1 mL sterile PBS to remove the unattached bacteria. Then, each CL was transferred to a sterile tube with 2 mL of PBS and was vortexed for 3 min and incubated 15 min in the US bath at 35 % amplitude to detach the bacteria from the material. Finally, the content of the tubes was serially diluted and plated in LB agar.

2.11. Cytotoxicity assessment of the coated CLs

The toxicity of the CLs was tested towards HCE cells H-6048IM. CLs were introduced in 24 well plate containing 10^5 of previously cultured cells in each well in 1 mL of DMEM. After 24 h, the composites were discarded from the media and the cellular viability was measured using alamarBlue® assay kit. At the same time, microscopy images of the cells were taken. The cells of each well were treated for 15 min with a 100 μL of a PBS mixture containing 0.1 % (v/v) of calcein AM and 0.1 % (v/v) of ethidium homodimer-1. A fluorescence microscope (Nikon/Eclipse Ti–S, The Netherlands) was employed to examine the stained cells, displayed in green for live cells and in red for dead ones.

2.12. Statistical analysis

All results are presented as mean values ± standard deviations (n = 3). One-way analysis of variance (ANOVA) and Post hoc Tukey test were performed to analyze the results statistically with Graph Pad Prism Software 5.04. P values less than 0.05 were considered statistically significant. One asterisk corresponds to $p < 0.05$, two asterisks to $p < 0.01$ and three asterisks to $p < 0.001$.

3. Results and discussion

3.1. Characterization of the NGs

The modified HA was analyzed by FTIR to confirm the successful grafting of ADH onto the polymer chain. The HA-ADH spectrum presented differences from the one of the pristine HA. The signal at ~3300 cm^{-1} increased, which may indicate the presence of new N-H bonds. Furthermore, a new signal appeared at ~2900 cm^{-1} corresponding to the C-H stretching in ADH. Additionally, the spectrum of the modified HA revealed the presence of amide signals, I at ~1637 cm^{-1} and II at ~1544 cm^{-1} (Fig. 1A) [40].

This functionalization allowed the HA to form a complex with cobalt ions, leading to the formation of a pink-colored precipitate characteristic of Co(II) compounds. In comparison with HA-ADH IR spectrum, the signal corresponding to the amide band I decreased, indicating that the $–NH_2$ groups participated in the complex. In addition, the signal between 3000 and 3600 cm^{-1} became broader, which has been correlated with the participation of –OH and –NH groups in the metal coordination

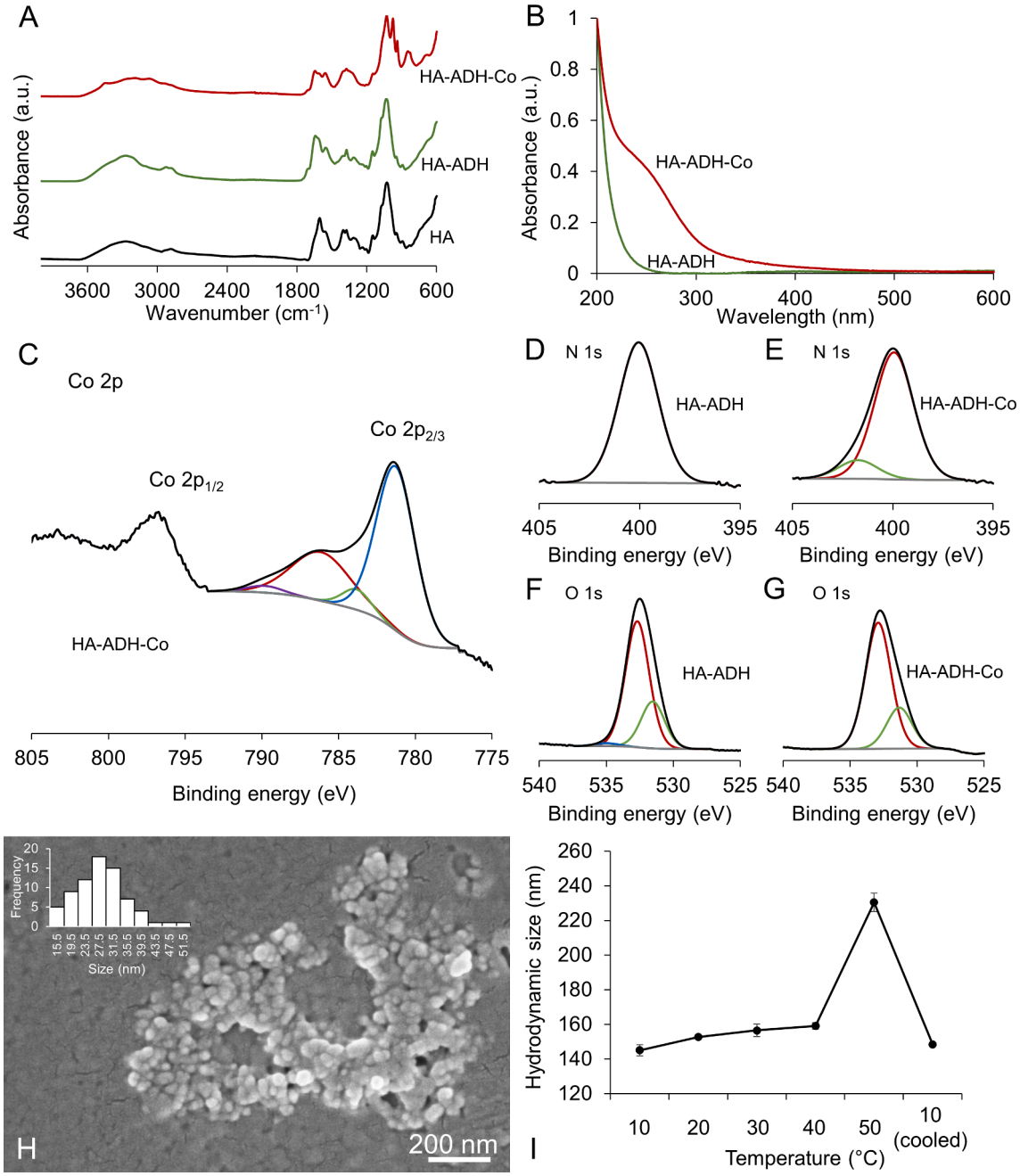

Fig. 1. NGs characterization. A) FTIR spectra of unmodified HA, ADH-modified HA (HA-ADH) and HA-ADH-Co NGs. B) UV–vis spectra of the modified polymer HA-ADH and the metal-polymer complex HA-ADH-Co. XPS spectra of Co2p for HA-ADH-Co (C), N1s for HA-ADH (D) and HA-ADH-Co (E), and O1s for HA-ADH (F) and HA-ADH-Co (G). H) SEM image of the NGs. I) Swelling of the NGs as a function of the temperature.

and hydrogen bond effects (Fig. 1A) [41]. Furthermore, the UV–vis spectra of the NGs displayed a signal below 370 nm that has been previously assigned to the interaction between the Co(II) and an organic ligand [42], producing a minor overlap and negligible effect in the range of human sight (Fig. 1B). The complex formation was also corroborated by XPS. The NGs presented an atomic composition of 59.7 % C, 7.6 % N, 31.2 % O and 1.6 % Co, whereby Co was identified by two broad signals at 781.5 and 796.8 eV, together with one of the satellite signals at 786.8 eV, in the Co_{2p} spectrum. The two spin orbit doublets signals assigned to $Co_{2p(1/2)}$ and $Co_{2p(3/2)}$ were compatible with Co^{2+}-ligand structures, confirming the presence of Co(II) ions in the sample (Fig. 1C) [43]. In parallel, the N1s spectrum of the modified polymer displayed a signal at 400 eV that corresponded to $–NH_2$ and –NH– groups. After the coordination with the cobalt ions, this signal decreased, and a new signal appeared at 402.8 eV (Fig. 1D and E). Co ions also led to the disappearance of the peak at 535.5 eV in the O1s spectrum, which has been previously reported for ADH complexes with copper (Fig. 1F and G) [44].

In order to further transform this complex into a NG, high-intensity US was applied for 30 min. Previous reports have explored the nanoformulation of insoluble and dispersible materials, such as biomass powder through US-assisted fragmentation, where the cavitation caused collisions and disintegration of aggregates [44]. The same approach was used to nanotransform HA-ADH-Co. Indeed, SEM revealed quasi-spherical structures between 20 and 30 nm (Fig. 1H). Subsequently, the ability of the NGs to alter their swelling capacity with temperature was estimated by dynamic light scattering (DLS). The hydrodynamic diameter of the NGs gradually increased with increasing temperature (10 °C–50 °C), from about 140 nm to 230 nm. After being cooled down back to 10 °C, the nanocomposite size returned to its initial value (Fig. 1I). These changes were ascribed to expansion of the porous NGs and water uptake upon heating, characteristic for NGs [45].

3.2. Antimicrobial characterization of the NGs

Before using the HA-ADH-Co NGs as coatings, their antibacterial activity against *S. aureus* and *P. aeruginosa* (both frequently encountered in eye infections) was tested in a colloidal form, i.e. in suspension. The NGs were able to kill both bacteria, reducing their concentration by 4.2 and 1.8 logs, respectively (i.e., more than 99.99 and 98.5 % of their populations) at 65 ppm cobalt content (Fig. 2A). Although some forms of cobalt have demonstrated antimicrobial activity, in particular Co(III) complexes, there is little information about the antimicrobial activity of Co(II) nanocomplexes. To study the possible interactions of the NGs with bacterial membranes, surface pressure-area isotherms were recorded on a model phospholipid monolayer, formed using the two main components of gram-negative membranes PE and PG. The PE:PG π-A isotherm increased until reaching collapse pressure of ~48 mN/m (Fig. 2B) [46]. The isotherm recorded with NGs alone showed a low surface pressure at larger areas that rapidly increased at lower compression areas, arriving to a collapse pressure of ~57.4 mN/m (Fig. 2C). This indicated that NGs may effectively disturb and collapse bacterial membranes. Furthermore, the isotherm shifted towards higher values when the NGs were present in the subphase. The model membrane achieved its physiological pressure of 33 mN/m at an area value of 83.9 $Å^2$/molecule, compared to the pristine subphase, which reached this pressure at an area of 62.1 $Å^2$/molecule (Fig. 2B). This further confirmed an interaction with or intercalation of the NGs with the model membrane, similar to the reported effect of HA-ADH [34].

Moreover, the nanocomposites were able to inhibit bacterial respiration. At 65 ppm cobalt, the activity of the bacterial NADH dehydrogenase was reduced by approximately 43 % and 27 % in the case of *P. aeruginosa* and *S. aureus*, respectively, after 2 h incubation (Fig. 2D). This effect has been ascribed to complexation of cobalt with amino groups on catalytic residues, leading to a metabolic failure of the cell

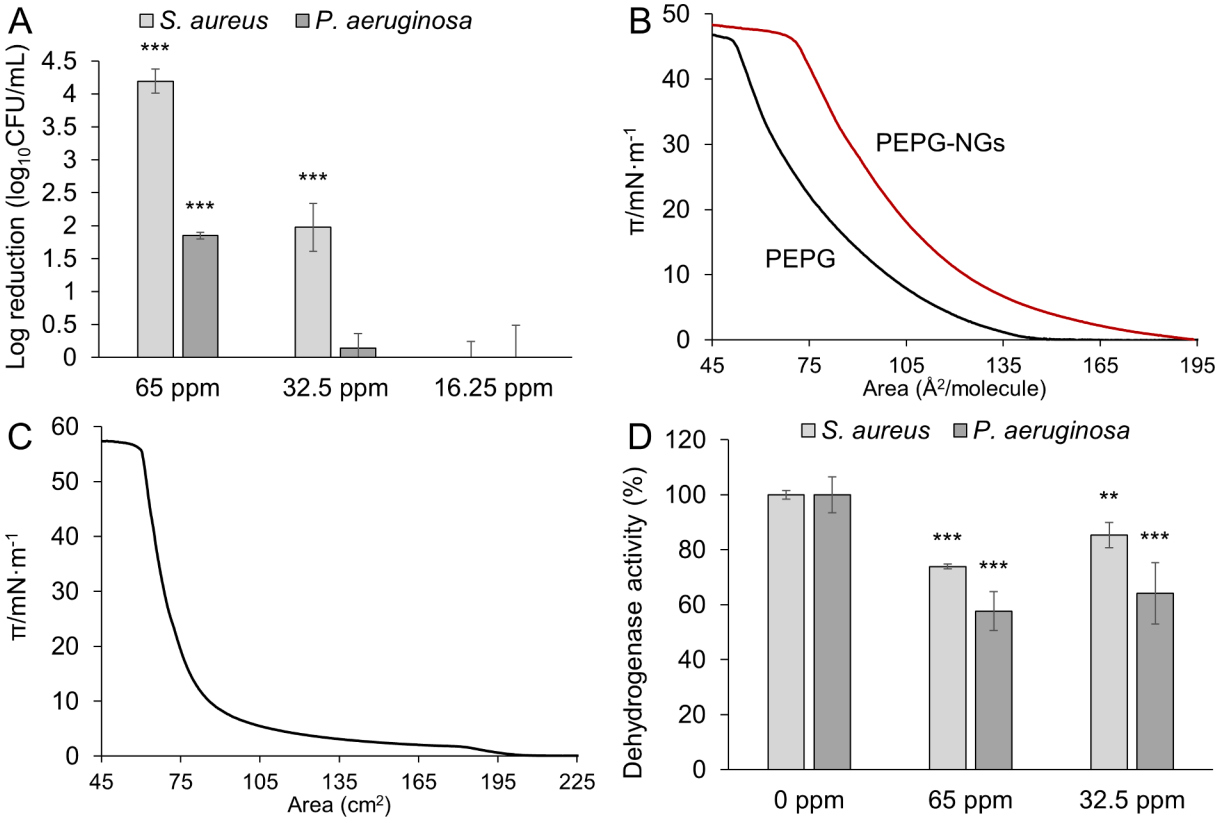

Fig. 2. A) Antibacterial activity of the NGs towards *S. aureus* (grey) and *P. aeruginosa* (dark grey). The log reduction values were calculated from the control bacteria without NGs corresponding to 6.3 and 5.8 $\log_{10}$CFU·mL^{-1}, respectively. B) π-A isotherm of a PE:PG mix monolayer in PBS subphase (solid), and in NGs subphase (dash). C) π-A isotherm of a NGs subphase without lipids. D) Dehydrogenase activity of *S. aureus* (grey) and *P. aeruginosa* (dark grey) after treatment with NGs for 2 h.

[47,48]. Altogether, these results demonstrate the multiple antimicrobial mechanisms of the NGs, acting both on the membrane and the metabolism, and pinpoint their future potential.

3.3. Characterization of the NGs coatings

Next, the NGs were simultaneously formed and coated on the CL surface using a one-step US-assisted approach. SEM images revealed uniform deposition of submicron aggregates (Fig. 3A and B), while the root mean square roughness (Rq) extracted from AFM images increased from less than 3 nm for the untreated CLs to about 19 nm for the coated CLs (Fig. 3C and D) due to their nanocomposite structure. Note that this nominal increase of roughness still lies in the low nm range and is thus not relevant for the wearing comfort [49].

Afterwards, the amount of cobalt in the CLs and its release related to the coating stability, was evaluated using ICP-MS. The amount of cobalt in the coating was assessed resulting in 1.6 ± 0.14 μg of cobalt/mg of dried CL. Following a 7-day incubation in PBS at pH 7.4, the cobalt concentration in the media rapidly increased, liberating 10 % of the total load after 30 min. Subsequently, the kinetics slowed down and became concentration-independent, maintaining about 50 % of residual cobalt loading after a week (Fig. 3E).

Finally, the potential interference on oxygen transport was measured via in-house electrochemical setup by linear sweep voltammetry. First, negative and positive controls for the oxygen reduction reaction (ORR) in the electrode chamber were established by purging N_2 through the solution and aeration by shaking, respectively. Mounting the CL samples resulted in reduced ORR currents in the limiting region due the additional mass transfer barrier, yet the pristine and the coated CLs performed virtually the same (Fig. 3F).

3.4. Optical and comfort properties of the coated CL

One of the main concerns regarding the coating of optical materials is the potential interference with the optical properties and their impact on wearer comfort. To address these issues, five different CLs were tested: the pristine CLs, CLs sonicated in water, HA-ADH solution or cobalt salt solution, and the one coated with NGs. The optic power of the pristine CL according to the manufacturer was −5, while the measurements in dry conditions yielded values around −5.16. Variations in a similar range were observed for all coated samples (Fig. 4A), indicating that the nanoscale coating did not significantly influence the lens thickness or

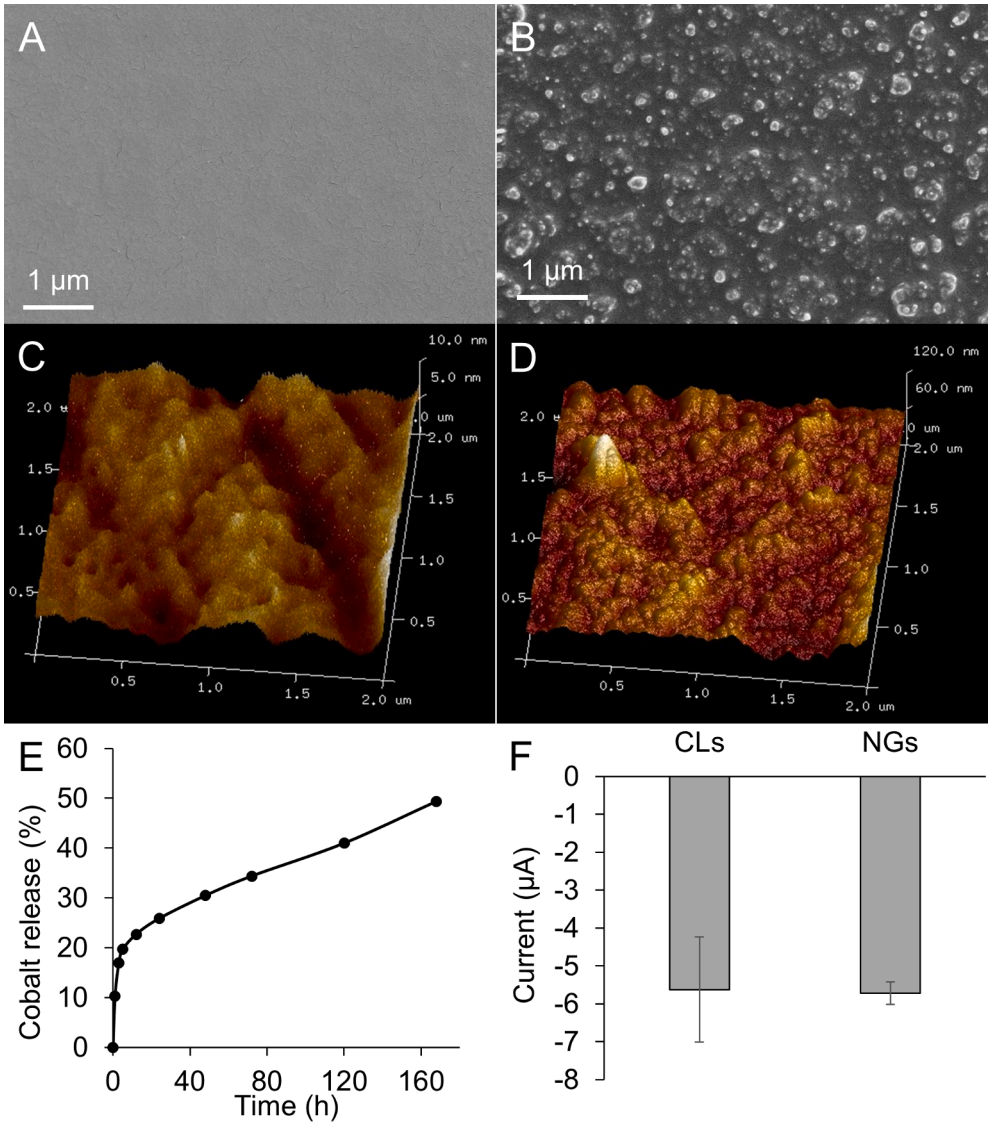

Fig. 3. NGs coating characterization. SEM images of the pristine (A) and NGs-coated CLs (B). AFM images of the pristine (C) and the NGs-coated CLs (D). E) Cobalt release incubated in PBS. F) ORR current at −0.5 V using CLs as membranes.

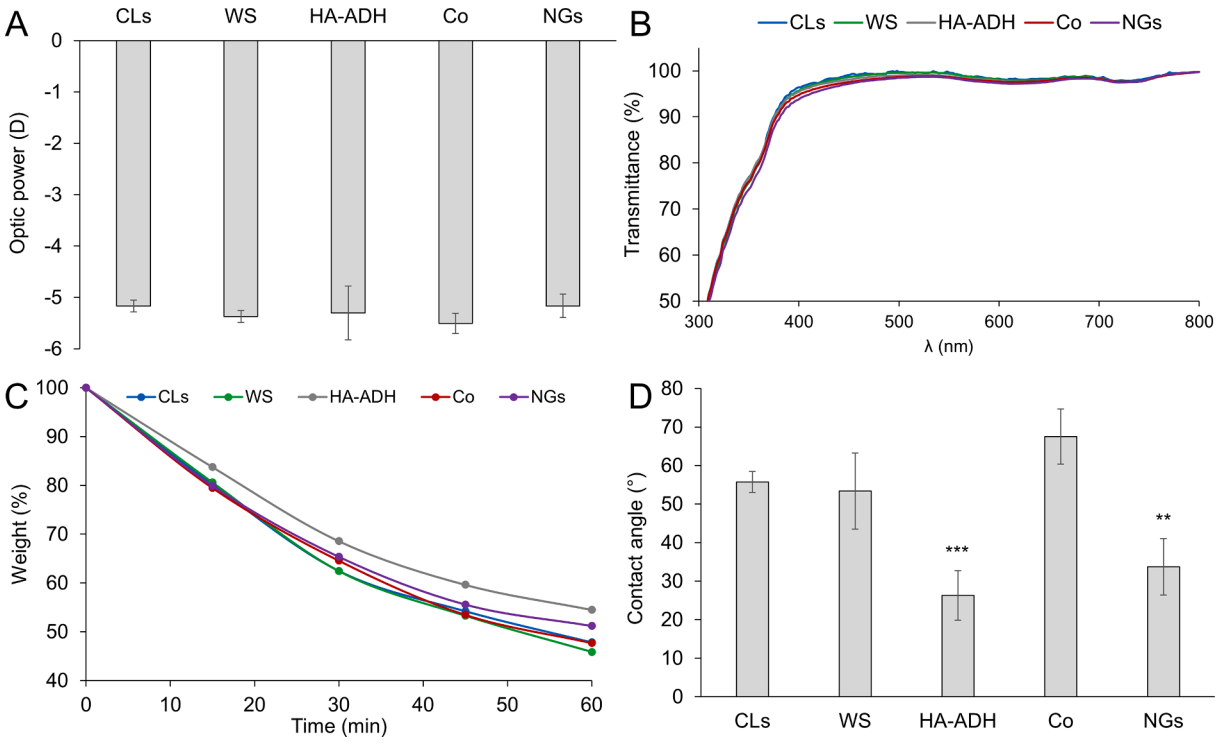

Fig. 4. Optic power (A), transmittance spectra (B), water loss (C) and contact angle (D) of pristine CLs (CLs), water sonicated CLs (WS), CLs coated with HA-ADH, CLs sonicated in the presence of Co(II) (Co) and the ones coated with NGs.

shape. Another key concern was the potential blockage of light transmission, however, all treated CLs exhibited similar transmittance values in the entire visible range (Fig. 4B), e.g., the variation at 550 nm was around 1 %, which agreed well with the featureless UV–vis spectrum of the NGs.

To evaluate if the comfort-related properties of the coated CLs were preserved, the water retention capability of the lenses was assessed next. During the dehydration test, the CLs sonicated in water exhibited the most rapid weight loss, potentially indicating some damage to the CL surface caused by the sonication process. On the other hand, the CLs coated with HA-ADH demonstrated slower dehydration, attributed to the well-known humectant properties of HA [50], which behavior was mirrored by the NG coating too (Fig. 4C) and corresponded to the reported enhanced wettability after deposition of HA [51,52]. Additionally, the contact angles of the different CLs were measured to confirm the humidifying role of HA-ADH in the NGs composition. The pristine CLs displayed a contact angle similar to the CLs sonicated in water, while the CLs sonicated in the presence of cobalt salt showed increased hydrophobicity, possibly due to cobalt aggregates on the silicone surface. Lastly, the CLs sonicated with HA-ADH and NGs exhibited reduced contact angles of 26° and 34°, respectively (Fig. 4D) indicating improved hydrophilicity, a property crucial to reduce dryness and eye irritation [12,53,54].

3.5. Protein adsorption on the CLs surface

Among the tear components that can adhere to the CL such as like lipids, mucins, and proteins, the latter are the most common deposit on soft CLs and their presence can lead to irritations and complications such as giant papillary conjunctivitis [55]. This is why the prevention of protein adsorption on the NG coating was assessed using BSA at the same concentration as the total protein content of human tears, and lysozyme at its tear concentration [56]. Approximately 0.6 mg BSA/cm^2 was absorbed onto the surface of the pristine CLs, which value was taken as a reference. The CLs sonicated in water and in cobalt salt solution exhibited fairly similar protein amounts on their surfaces, while the coatings based on HA-ADH reduced the adsorption by 80 % when bulk polymer was used and by 60 % for the NGs (Fig. 5A). This effect was ascribed to electrostatic repulsion because both HA and BSA are negatively charged under physiological conditions. On the other hand, 0.16 mg lysozyme/cm^2, a positively charged protein that represents almost 40 % of the total protein content in human tears, were attached to pristine CL. In this case, the CLs coated with modified HA exhibited increased adsorption, while the presence of positively charged Co^{2+} in the sonication media decreased the lysozyme amount, which corroborated the hypothesis for electrostatic interactions, in this case attraction. Yet, surprisingly, the NG coating led to the lowest lysozyme adsorption (Fig. 5A), which suggested that other effects are in place. First, some nanogels have been reported to form a hydration layer that reduces the fouling [57]. Additionally, the initial burst release of cobalt ions from the NGs might have also affected the lysozyme adsorption because the latter is reduced in presence of salts [58,59].

3.6. Bacterial adhesion on CLs surface

Next, the shielding against bacterial colonization was assessed by incubation with *S. aureus* and *P. aeruginosa*. The pristine CL, the one sonicated in water, and the one coated with HA-ADH presented similar values of bacterial loading. On the other hand, the CLs sonicated with cobalt salts hindered the adhesion of both pathogens by about 2 logs, which effect has been previously ascribed to reduced viability [60]. Importantly, the shielding was potentiated by the NGs, reducing *S. aureus* and *P. aeruginosa* by 3.2 and 2.7 logs respectively (Fig. 5B). This was likely due to a higher loading of cobalt in NG form on the surface, which also endowed it with additional antifouling activity. Thus, the HA-ADH-Co NGs simultaneously killed bacteria and hindered their adhesion, altogether reducing the cell concentration on the CLs and preventing subsequent formation of biofilms.

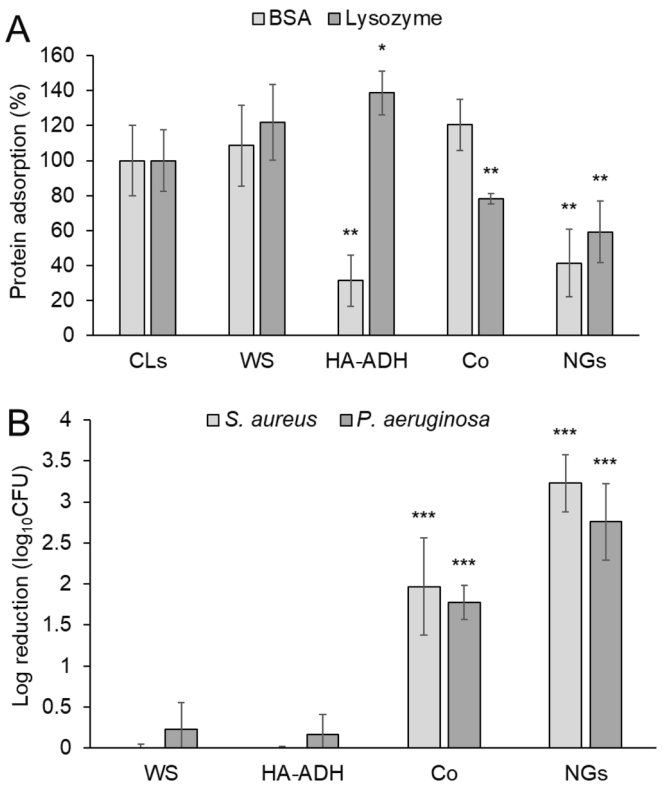

Fig. 5. Protein and bacterial adhesion to pristine CLs (CLs), CL sonicated with water (WS), sonicated with HA-ADH, sonicated in the presence of Co(II) (Co) and sonicated with NGs. A) BSA (grey) and lysozyme (dark grey) adherence onto the CL surface and B) Adhesion of *S. aureus* (grey) and *P. aeruginosa* (dark grey) to CLs surface. The reduction of bacterial was calculated regarding the amount of bacteria grown on the pristine CLs corresponding to 3.9 (*S. aureus*) and 4.8 (*P. aeruginosa*) logs respectively.

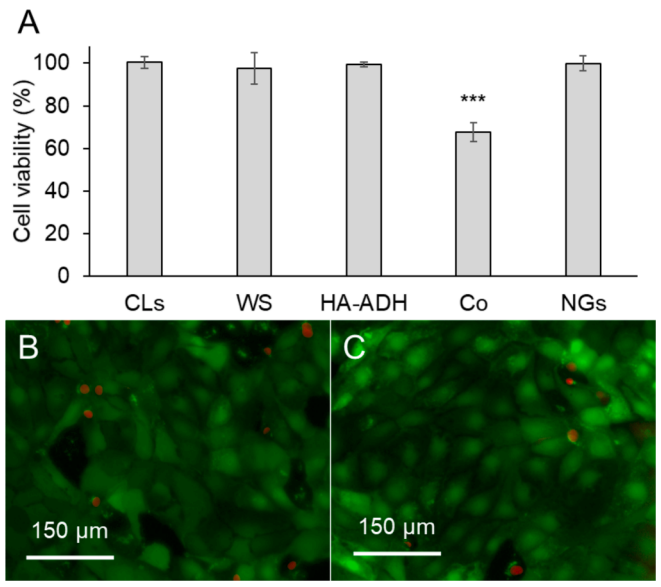

Fig. 6. Cytotoxicity assessment of the NGs coatings. A) alamarBlue assay for cellular metabolic activity of HCE cells H-6048IM after 24 h of incubation with the pristine CLs (CLs), CL sonicated with water (WS), sonicated with HA-ADH, sonicated in the presence of Co(II) (Co) and sonicated with NGs. Fluorescence microscopy images of HCE cells H-6048IM after 24 h of incubation with pristine (B) and NGs-coated (C) CLs.

3.7. Cytotoxicity assessment

To evaluate the cytotoxicity of the coatings, human epithelial corneal cells were incubated with the CLs for 24 h. The pristine CL served as the reference for cellular viability. The samples sonicated in water and HA-ADH demonstrated viabilities above 95 % compared to the control, while the CLs sonicated with cobalt salts exhibited reduced viability. Yet, NGs coating restored the biocompatibility to almost 100 % (Fig. 6A), corroborating the well-known attenuating effect of biopolymers on metal toxicity and they exhibited no harmful effects on human corneal cells, similar to the commercial material. Additionally, fluorescence images showed no substantial differences in cell density, morphology, or color regarding the cells incubated with the pristine and the coated CLs (Fig. 6B and C).

4. Conclusions

Among the various medical devices in closer contact with the human body that would benefit from enhanced antimicrobial properties, CLs present distinct design challenges associated with the delicate ocular environment and the additional optical requirements. The silicone hydrogel coating developed in this work, based on nanogels of modified hyaluronic acid and cobalt complexes, appears to fulfill these requisites, while preventing unspecific biomolecule adsorption and bacterial colonization. Said coating efficiently shielded from relevant Gram-positive and Gram-negative pathogens without inducing toxicity to human cells. Moreover, HA improved the wettability, while dioptric power or light transmittance were not affected. Importantly, the coating was formed by a facile sonochemical procedure, which could be potentially integrated in existing production lines. These results suggest that the novel hybrid NG coatings represent a viable alternative to the existing biocidal treatment of CLs for bacterial infection prevention.

CRediT authorship contribution statement

Guillem Ferreres: Writing – original draft, Software, Methodology, Investigation, Conceptualization. **Sílvia Pérez-Rafael:** Writing – original draft, Supervision, Software, Methodology, Investigation. **Ester Guaus:** Methodology, Conceptualization. **Òscar Palacios:** Methodology, Data curation. **Ivan Ivanov:** Writing – review & editing, Supervision, Methodology, Conceptualization. **Juan Torrent-Burgués:** Writing – review & editing, Supervision, Methodology, Formal analysis, Conceptualization. **Tzanko Tzanov:** Writing – review & editing, Writing – original draft, Supervision, Project administration, Funding acquisition, Conceptualization.

Declaration of competing interest

The authors declare that they have no known competing financial interests or personal relationships that could have appeared to influence the work reported in this paper.

Acknowledgments

This work was supported by Spanish Ministry of Economy and Competitiveness Projects (MINECO) CoatToSave—Nanoenabled hydrogel coatings against antimicrobial-resistant catheter-related infections (PID2019-104111RB-I00) and NANOGErida – Self-assembled nanoenabled hydrogels targeting multiple chronicity factors in wounds (PID2022-142229OB-I00). G. F. acknowledges Universitat Politècnica de Catalunya and Banco Santander for his PhD grant (113 FPI-UPC 2018). T.T. acknowledges ICREA Academia 2021-07 for excellence in research funded by the Generalitat de Catalunya.

References

[1] D.S. Jacobs, K.G. Carrasquillo, P.D. Cottrell, F.J. Fernández-Velázquez, R. Gil-Cazorla, I. Jalbert, A.D. Pucker, K. Riccobono, D.M. Robertson, L. Szczotka-Flynn, L. Speedwell, F. Stapleton, CLEAR – medical use of contact lenses, Contact Lens. Anterior Eye 44 (2021) 289–329, https://doi.org/10.1016/j.clae.2021.02.002.

[2] F.A. Maulvi, T.G. Soni, D.O. Shah, A review on therapeutic contact lenses for ocular drug delivery, Drug Deliv. 23 (2016) 3017–3026, https://doi.org/10.3109/10717544.2016.1138342.

[3] A. Mahomed, J.S. Wolffsohn, B.J. Tighe, Structural design of contact lens-based drug delivery systems; in vitro and in vivo studies of ocular triggering mechanisms, Contact Lens. Anterior Eye 39 (2016) 97–105, https://doi.org/10.1016/j.clae.2015.07.007.

[4] E. Caló, V.V. Khutoryanskiy, Biomedical applications of hydrogels: a review of patents and commercial products, Eur. Polym. J. 65 (2015) 252–267, https://doi.org/10.1016/j.eurpolymj.2014.11.024.

[5] B.J. Tighe, A decade of silicone hydrogel development: surface properties, mechanical properties, and ocular compatibility, Eye Contact Lens. 39 (2013) 4–12, https://doi.org/10.1097/ICL.0b013e318275452b.

[6] J.T. Jacob, Biocompatibility in the development of silicone-hydrogel lenses, Eye Contact Lens. 39 (2013) 13–19, https://doi.org/10.1097/ICL.0b013e31827dbb00.

[7] J. Pozuelo, V. Compañ, J.M. González-Méijome, M. González, S. Mollá, Oxygen and ionic transport in hydrogel and silicone-hydrogel contact lens materials: an experimental and theoretical study, J. Membr. Sci. 452 (2014) 62–72, https://doi.org/10.1016/j.memsci.2013.10.010.

[8] D. Dutta, N. Cole, M. Willcox, Factors influencing bacterial adhesion to contact lenses, Mol. Vis. 18 (2012) 14–21.

[9] Y.W. Ibrahim, D.L. Boase, I.A. Cree, How could contact lens wearers be at risk of Acanthamoeba infection? A review, J. Optom. 2 (2009) 60–66, https://doi.org/10.3921/joptom.2009.60.

[10] S. Tuft, T.F. Somerville, J.P.O. Li, T. Neal, S. De, M.J. Horsburgh, J.L. Fothergill, D. Foulkes, S. Kaye, Bacterial keratitis: identifying the areas of clinical uncertainty, Prog. Retin. Eye Res. 89 (2022) 101031, https://doi.org/10.1016/j.preteyeres.2021.101031.

[11] M. Cabrera-Aguas, P. Khoo, S.L. Watson, Infectious keratitis A review, Clin. Exp. Ophthalmol. 50 (2022) 543–562, https://doi.org/10.1111/ceo.14113.

[12] J.S. Bertino, Impact of antibiotic resistance in the management of ocular infections: the role of current and future antibiotics, Clin. Ophthalmol. 3 (2009) 507–521, https://doi.org/10.2147/opth.s5778.

[13] S.M. Mathews, J.E. Spallholz, M.J. Grimson, R.R. Dubielzig, T. Gray, T.W. Reid, Prevention of bacterial colonization of contact lenses with covalently attached selenium and effects on the rabbit cornea, Cornea 25 (2006) 806–814, https://doi.org/10.1097/01.ico.0000224636.57062.90.

[14] A. Rai, S. Pinto, M.B. Evangelista, H. Gil, S. Kallip, M.G.S. Ferreira, L. Ferreira, High-density antimicrobial peptide coating with broad activity and low cytotoxicity against human cells, Acta Biomater. 33 (2016) 64–77, https://doi.org/10.1016/j.actbio.2016.01.035.

[15] H. Zhu, A. Kumar, J. Ozkan, R. Bandara, A. Ding, I. Perera, P. Steinberg, N. Kumar, W. Lao, S.S. Griesser, L. Britcher, H.J. Griesser, M.D.P. Willcox, Fimbrolide-coated antimicrobial lenses: their in vitro and in vivo effects, Optom. Vis. Sci. 85 (2008) 292–300, https://doi.org/10.1097/OPX.0b013e31816bea0f.

[16] A. Xiao, C. Dhand, C.M. Leung, R.W. Beuerman, S. Ramakrishna, R. Lakshminarayanan, Strategies to design antimicrobial contact lenses and contact lens cases, J. Mater. Chem. B 6 (2018) 2171–2186, https://doi.org/10.1039/c7tb03136j.

[17] L. Ma, K. Li, J. Xia, C. Chen, Y. Liu, S. Lang, L. Yu, G. Liu, Commercial soft contact lenses engineered with zwitterionic silver nanoparticles for effectively treating microbial keratitis, J. Colloid Interface Sci. 610 (2022) 923–933, https://doi.org/10.1016/j.jcis.2021.11.145.

[18] L.M. Shaker, A. Alamiery, M. Takriff, W.N.R. Wan Isahak, Novel blue-wavelength-blocking contact lens with er3+/tio2 nps: manufacture and characterization, Nanomaterials 11 (2021) 1–12, https://doi.org/10.3390/nano11092190.

[19] G. Liu, K. Li, H. Wang, L. Ma, L. Yu, Y. Nie, Stable fabrication of zwitterionic coating based on copper-phenolic networks on contact lens with improved surface wettability and broad-spectrum antimicrobial activity, ACS Appl. Mater. Interfaces 12 (2020) 16125–16136, https://doi.org/10.1021/acsami.0c02143.

[20] F. Gomollón-Bel, IUPAC top ten emerging technologies in chemistry 2021, Chem. Int. 43 (2021) 13–20, https://doi.org/10.1515/ci-2021-0404.

[21] J. Hoyo, K. Ivanova, E. Guaus, T. Tzanov, Multifunctional ZnO NPs-chitosan-gallic acid hybrid nanocoating to overcome contact lenses associated conditions and discomfort, J. Colloid Interface Sci. 543 (2019) 114–121, https://doi.org/10.1016/j.jcis.2019.02.043.

[22] Y. Nahum, R. Israeli, G. Mircus, I. Perelshtein, M. Ehrenberg, S. Gutfreund, A. Gedanken, I. Bahar, Antibacterial and physical properties of a novel sonochemical-assisted Zn-CuO contact lens nanocoating, Graefe's Arch. Clin. Exp. Ophthalmol. 257 (2019) 95–100, https://doi.org/10.1007/s00417-018-4172-9.

[23] S.A. Khan, S. Shahid, T. Mahmood, C.S. Lee, Contact lenses coated with hybrid multifunctional ternary nanocoatings (Phytomolecule-coated ZnO nanoparticles: Gallic Acid:Tobramycin) for the treatment of bacterial and fungal keratitis, Acta Biomater. 128 (2021) 262–276, https://doi.org/10.1016/j.actbio.2021.04.014.

[24] G.R. Tortella, O. Rubilar, N. Durán, M.C. Diez, M. Martínez, J. Parada, A.B. Seabra, Silver nanoparticles: toxicity in model organisms as an overview of its hazard for human health and the environment, J. Hazard. Mater. 390 (2020) 121974, https://doi.org/10.1016/j.jhazmat.2019.121974.

[25] T. Ameh, C.M. Sayes, The potential exposure and hazards of copper nanoparticles: a review, Environ. Toxicol. Pharmacol. 71 (2019) 103220, https://doi.org/10.1016/j.etap.2019.103220.

[26] R.P. Sharma, S.D. Raut, R.M. Mulani, A.S. Kadam, R.S. Mane, Sol–gel auto-combustion mediated cobalt ferrite nanoparticles: a potential material for antimicrobial applications, Int. Nano Lett. 9 (2019) 141–147, https://doi.org/10.1007/s40089-019-0268-4.

[27] H.A. Zaman, S. Sharif, D.W. Kim, M.H. Idris, M.A. Suhaimi, Z. Tumurkhuyag, Machinability of cobalt-based and cobalt chromium molybdenum alloys – a review, Proc. Manuf. 11 (2017) 563–570, https://doi.org/10.1016/j.promfg.2017.07.150.

[28] R.J. Coffey, J.C. Flickinger, D.J. Bissonette, L.D. Lunsford, Radiosurgery for solitary brain metastases using the cobalt-60 gamma unit: methods and results in 24 patients, Int. J. Rad. Oncol. Biol. Phys. 17 (1991) 823–827, https://doi.org/10.1016/0360-3016(91)90240-5.

[29] J.H. Jiang, Y.H. Lei, X. Li, Y. Pi, H. Zhu, Q.G. Li, C.H. Li, New cobalt(II) Schiff base complex: synthesis, characterization, DFT calculation and antimicrobial activity, Inorg. Chem. Commun. 127 (2021) 108350, https://doi.org/10.1016/j.inoche.2020.108350.

[30] L. Leyssens, B. Vinck, C. Van Der Straeten, F. Wuyts, L. Maes, Cobalt toxicity in humans—a review of the potential sources and systemic health effects, Toxicology 387 (2017) 43–56, https://doi.org/10.1016/j.tox.2017.05.015.

[31] B.B. Karakocak, J. Iang, P. Biswas, N. Ravi, Hyaluronate coating enhances the delivery and biocompatibility of gold nanoparticles, Carbohydr. Polym. 186 (2019) 243–251, https://doi.org/10.1016/j.carbpol.2018.01.046.Hyaluronate.

[32] Q. Sun, H. Bi, Z. Wang, C. Li, X. Wang, J. Xu, H. Zhu, R. Zhao, F. He, S. Gai, P. Yang, Hyaluronic acid-targeted and pH-responsive drug delivery system based on metal-organic frameworks for efficient antitumor therapy, Biomaterials 223 (2019) 119473, https://doi.org/10.1016/j.biomaterials.2019.119473.

[33] S. Pérez-Rafael, K. Ivanova, I. Stefanov, J. Puiggalí, L.J. del Valle, K. Todorova, P. Dimitrov, D. Hinojosa-Caballero, T. Tzanov, Nanoparticle-driven self-assembling injectable hydrogels provide a multi-factorial approach for chronic wound treatment, Acta Biomater. 134 (2021) 131–143, https://doi.org/10.1016/j.actbio.2021.07.020.

[34] G. Ferreres, S. Pérez-Rafael, J. Torrent-Burgués, T. Tzanov, Hyaluronic acid derivative molecular weight-dependent synthesis and antimicrobial effect of hybrid silver nanoparticles, Int. J. Mol. Sci. 22 (2021) 13428, https://doi.org/10.3390/ijms222413428.

[35] A. Huynh, R. Priefer, Hyaluronic acid applications in ophthalmology, rheumatology, and dermatology, Carbohydr. Res. 489 (2020) 107950, https://doi.org/10.1016/j.carres.2020.107950.

[36] N.M. Salwowska, K.A. Bebenek, D.A. Żądło, D.L. Wcisło-Dziadecka, Physiochemical properties and application of hyaluronic acid: a systematic review, J. Cosmet. Dermatol. 15 (2016) 520–526, https://doi.org/10.1111/jocd.12237.

[37] A.S. Sonzogni, S. Hamzehlou, V.D.G. Gonzalez, J.R. Leiza, R.J. Minari, Multilobular morphology: the key for biphase multifunctional nanogels, Soft Matter 17 (2021) 9353–9362, https://doi.org/10.1039/d1sm00968k.

[38] S. Kwang, J. Kyu, T. Tomimatsu, T. Shimoboji, Synthesis and degradation test of hyaluronic acid hydrogels, Int. J. Biol. Macromol. 40 (2007) 374–380, https://doi.org/10.1016/j.ijbiomac.2006.09.019.

[39] A. Jarboui, Y. Holade, J.P. Mericq, C. Charmette, T. Thami, P. Biermans, S. Tingry, D. Bouyer, Electroanalytical assessment of the oxygen permeability at the gas-solid-liquid interface in polymer-based materials for lens applications, ChemElectroChem 7 (2020) 4879–4888, https://doi.org/10.1002/celc.202001160.

[40] E. Zheng, Q. Dang, C. Liu, B. Fan, J. Yan, Z. Yu, H. Zhang, Preparation and evaluation of adipic acid dihydrazide cross-linked carboxymethyl chitosan microspheres for copper ion adsorption, Colloids Surf. A Physicochem. Eng. Asp. 502 (2016) 34–43, https://doi.org/10.1016/j.colsurfa.2016.05.003.

[41] A. Rogina, A. Lončarević, M. Antunović, I. Marijanović, M. Ivanković, H. Ivanković, Tuning physicochemical and biological properties of chitosan through complexation with transition metal ions, Int. J. Biol. Macromol. 129 (2019) 645–652, https://doi.org/10.1016/j.ijbiomac.2019.02.075.

[42] F.A. El-Saied, M.M.E. Shakdofa, A.S. El Tabl, M.M. Abd-Elzaher, N. Morsy, Coordination versatility of N2O4 polydentate hydrazonic ligand in Zn(II), Cu(II), Ni(II), Co(II), Mn(II) and Pd(II) complexes and antimicrobial evaluation, Beni Suef Univ. J. Basic Appl. Sci. 6 (2017) 310–320, https://doi.org/10.1016/j.bjbas.2017.09.005.

[43] M.C. Biesinger, B.P. Payne, A.P. Grosvenor, L.W.M. Lau, A.R. Gerson, R.S.C. Smart, Resolving surface chemical states in XPS analysis of first row transition metals, oxides and hydroxides: Cr, Mn, Fe, Co and Ni, Appl. Surf. Sci. 257 (2011) 2717–2730, https://doi.org/10.1016/j.apsusc.2010.10.051.

[44] S. Pérez-Rafael, G. Ferreres, R.W. Kessler, W. Kessler, J. Blair, G. Rathee, A. G. Morena, T. Tzanov, Continuous sonochemical nanotransformation of lignin – process design and control, Ultrason. Sonochem. 98 (2023) 106499, https://doi.org/10.1016/j.ultsonch.2023.106499.

[45] M. Ohshio, K. Ishihara, A. Maruyama, N. Shimada, S.I. Yusa, Synthesis and properties of upper critical solution temperature responsive nanogels, Langmuir 35 (2019) 7261–7267, https://doi.org/10.1021/acs.langmuir.9b00849.

[46] G. Ferreres, K. Ivanova, J. Torrent-Burgués, T. Tzanov, Multimodal silver-chitosan-acylase nanoparticles inhibit bacterial growth and biofilm formation by Gram-negative Pseudomonas aeruginosa bacterium, J. Colloid Interface Sci. 646 (2023) 576–586, https://doi.org/10.1016/j.jcis.2023.04.184.

[47] J. Wang, N.S. Nemeria, K. Chandrasekhar, S. Kumaran, P. Arjunan, S. Reynolds, G. Calero, R. Brukh, L. Kakalis, W. Furey, F. Jordan, Structure and function of the catalytic domain of the dihydrolipoyl acetyltransferase component in Escherichia

coli pyruvate dehydrogenase complex, J. Biol. Chem. 289 (2014) 15215–15230, https://doi.org/10.1074/jbc.M113.544080.
[48] M. Zaborowska, J. Kucharski, J. Wyszkowska, Biological activity of soil contaminated with cobalt, tin, and molybdenum, Environ. Monit. Assess. 188 (2016) 1–10, https://doi.org/10.1007/s10661-016-5399-8.
[49] C.F. Lai, F.J. Shiau, Enhanced and extended ophthalmic drug delivery by pH-triggered drug-eluting contact lenses with large-pore mesoporous silica nanoparticles, ACS Appl. Mater. Interfaces 15 (2023) 18630–18638, https://doi.org/10.1021/acsami.2c22860.
[50] S. Srinivasan, R. Garofalo, R. Williams, Safe and effective management of dry eye symptoms with hydroxypropyl guar and hyaluronic acid dual-polymer lubricating eye drops: a review of preclinical and clinical studies, Clin. Ophthalmol. 17 (2023) 3883–3898, https://doi.org/10.2147/OPTH.S428725.
[51] M. Korogiannaki, L. Jones, H. Sheardown, Impact of a hyaluronic acid-grafted layer on the surface properties of model silicone hydrogel contact lenses, Langmuir 35 (2019) 950–961, https://doi.org/10.1021/acs.langmuir.8b01693.
[52] F.A. Maulvi, M.B. Parmar, K.H. Shetty, A.R. Patel, B.V. Desai, B.A. Vyas, D.T. Desai, P. Kalaiselvan, S. Masoudi, D.O. Shah, M.D.P. Willcox, Role of micelle dynamics in enhancing cyclosporine uptake in hyaluronic acid-contact lenses for improved critical lens properties in dry eye management, Colloids Surf. A Physicochem. Eng. Asp. 688 (2024) 133550, https://doi.org/10.1016/j.colsurfa.2024.133550.
[53] K. Yamasaki, E. Drolle, H. Nakagawa, R. Hisamura, W. Ngo, L. Jones, Impact of a low molecular weight hyaluronic acid derivative on contact lens wettability, Cont. Lens Anterior Eye 44 (2021) 101334, https://doi.org/10.1016/j.clae.2020.05.003.
[54] C.C. Sun, Y.H. Chan, P.W. Huang, N.N. Chen, Evaluation of two artificial tears containing hyaluronic acid for post cataract surgery dry eye disease: a randomized controlled trial, Ophthalmol. Ther. (2024) 1–13, https://doi.org/10.1007/s40123-024-01015-9.
[55] S.E. Kenny, C.B. Tye, D.A. Johnson, A. Kheirkhah, Giant papillary conjunctivitis: a review, Ocular Surf. 18 (2020) 396–402, https://doi.org/10.1016/j.jtos.2020.03.007.
[56] J. Filik, N. Stone, Investigation into the protein composition of human tear fluid using centrifugal filters and drop coating deposition Raman spectroscopy, J. Raman Spectrosc. 40 (2009) 218–224, https://doi.org/10.1002/jrs.2113.
[57] D. Keskin, L. Tromp, O. Mergel, G. Zu, E. Warszawik, H.C. van der Mei, P. van Rijn, Highly efficient antimicrobial and antifouling surface coatings with triclosan-loaded nanogels, ACS Appl. Mater. Interfaces 12 (2020) 57721–57731, https://doi.org/10.1021/acsami.0c18172.
[58] H. Göhring, M. Paulus, P. Salmen, F. Wirkert, T. Kruse, P. Degen, S. Stuhr, H. Rehage, M. Tolan, Salt induced reduction of lysozyme adsorption at charged interfaces, J. Phys. Condens. Matter 27 (2015), https://doi.org/10.1088/0953-8984/27/23/235103.
[59] M.D.P. Willcox, N. Harmis, B.A. Cowell, T. Williams, B.A. Holden, Bacterial interactions with contact lenses; effects of lens material, lens wear and microbial physiology, Biomaterials 22 (2001) 3235–3247, https://doi.org/10.1016/S0142-9612(01)00161-2.
[60] S. Hatamie, M.M. Ahadian, M. Soufi Zomorod, S. Torabi, A. Babaie, S. Hosseinzadeh, M. Soleimani, N. Hatami, Z.H. Wei, Antibacterial properties of nanoporous graphene oxide/cobalt metal organic framework, Mater. Sci. Eng. C 104 (2019) 109862, https://doi.org/10.1016/j.msec.2019.109862.